

Calculating the rotational friction coefficient of fractal aerosol particles in the transition regime using extended Kirkwood-Riseman theory

James Corson,¹ George W. Mulholland,¹ and Michael R. Zachariah^{1,2,*}¹*Department of Chemical and Biomolecular Engineering, University of Maryland, College Park, Maryland 20742, USA*²*Department of Chemistry and Biochemistry, University of Maryland, College Park, Maryland 20742, USA*

(Received 31 March 2017; published 18 July 2017)

We apply our extended Kirkwood-Riseman theory to compute the translation, rotation, and coupling friction tensors and the scalar rotational friction coefficient for an aerosol fractal aggregate in the transition flow regime. The method can be used for particles consisting of spheres in contact. Our approach considers only the linear velocity of the primary spheres in a rotating aggregate and ignores rotational and coupling interactions between spheres. We show that this simplified approach is within approximately 40% of the true value for any particle for Knudsen numbers between 0.01 and 100. The method is especially accurate (i.e., within about 5%) near the free-molecule regime, where there is little interaction between the particle and the flow field, and for particles with low fractal dimension ($\lesssim 2$) consisting of many spheres, where the average distance between spheres is large and translational interaction effects dominate. Our results suggest that there is a universal relationship between the rotational friction coefficient and an aggregate Knudsen number, defined as the ratio of continuum to free-molecule rotational friction coefficients.

DOI: [10.1103/PhysRevE.96.013110](https://doi.org/10.1103/PhysRevE.96.013110)

I. INTRODUCTION

Nanoscale aerosol particles consisting of many spheres in point contact are formed in many natural and synthetic processes. The size, shape, and orientation of these particles greatly affect their transport properties [1,2], optical properties [3–5], degree of alignment in an external field [3–6], filtration efficiency [7], and their effects in biological systems, including lung deposition [8,9].

Much of the theoretical and experimental literature on the transport properties of nano-scale aerosol particles focuses on the translational friction coefficient (or, equivalently, the electrical mobility). There is comparatively little focus on the rotational friction or diffusion coefficients, which affect particle alignment in an external field and relaxation time from an aligned state to a fully random state [3–6]. Inclusion of rotational dynamics is also important when considering particle coagulation rates in Brownian motion simulations [10].

There are analytical expressions available in the literature for the torque on (or the rotational diffusion coefficient of) simple shapes—such as spheres, rods, and ellipsoids—in both the continuum [11–13] and free-molecule regimes [14–16]. However, there are no such expressions for complicated shapes such as fractal aggregates. Garcia de la Torre and colleagues have extensively studied the rotational problem for rigid particles consisting of multiple spheres in point contact in the continuum regime [17–21]. More will be said about their work shortly. There are far fewer studies available for the free-molecule regime. Li *et al.* [6] approximate the torque on a fractal aggregate rotating in a quiescent fluid by considering only the linear velocity of each sphere and neglecting the effects of shielding by the other spheres in the cluster, thereby providing an upper bound for the torque. We are unaware of any more detailed methods for calculating the torque on a fractal aggregate in either the free-molecule or the transition flow regime. This

is significant because in many aerosol applications the primary spheres are much smaller than the mean free path of the gas.

In this paper, we discuss the application of our extended Kirkwood-Riseman (EKR) theory [22] to the translational and rotational motion of fractal aggregates in the transition flow regime. In Sec. II we provide the equations for the drag and torque on a rigid particle, as introduced by Brenner [12]; we describe how one can apply Kirkwood-Riseman theory to the problem; and we employ Monte Carlo to compute the drag and torque on a translating or rotating particle, which we use to validate our EKR method. We present our results for the rotational friction coefficient as a function of Knudsen number and compare our results for $\text{Kn} \ll 1$ and $\text{Kn} \gg 1$ to the continuum and free-molecule limits in Sec. III.

II. DRAG AND TORQUE ON A RIGID PARTICLE

Consider a rigid particle with center of mass moving at velocity \mathbf{U}_O and rotating with angular velocity $\boldsymbol{\omega}$, where point O is the origin of the system. For particles in Stokes (i.e., low Reynolds number) flow, the force \mathbf{F} and torque \mathbf{T}_O on the particle are given by

$$\mathbf{F} = -\boldsymbol{\Xi}_t \cdot \mathbf{U}_O - \boldsymbol{\Xi}_{O,c}^\dagger \cdot \boldsymbol{\omega}, \quad (1)$$

$$\mathbf{T}_O = -\boldsymbol{\Xi}_{O,c} \cdot \mathbf{U}_O - \boldsymbol{\Xi}_{O,r} \cdot \boldsymbol{\omega}, \quad (2)$$

where $\boldsymbol{\Xi}_t$, $\boldsymbol{\Xi}_{O,r}$, and $\boldsymbol{\Xi}_{O,c}$ are the friction tensors for translation, rotation, and translation-rotation coupling, respectively, and $\boldsymbol{\Xi}_{O,c}^\dagger$ is the transpose of the coupling tensor. The coupling and rotation tensors are defined with respect to the origin, O , while the translation tensor is independent of the origin.

Brenner [12] proved that these friction tensors are related to the translation, rotation, and coupling diffusion tensors by the generalized Stokes-Einstein relation

$$\mathcal{D}_O = kT \mathcal{M}_O^{-1}, \quad (3)$$

*mrz@umd.edu

where \mathcal{D}_O and \mathcal{M}_O are the 6×6 grand diffusion and friction matrices given by

$$\mathcal{D}_O = \begin{bmatrix} \mathbf{D}_{O,t} & \mathbf{D}_{O,c}^\dagger \\ \mathbf{D}_{O,c} & \mathbf{D}_r \end{bmatrix}, \quad (4)$$

$$\mathcal{M}_O = \begin{bmatrix} \boldsymbol{\Xi}_t & \boldsymbol{\Xi}_{O,c}^\dagger \\ \boldsymbol{\Xi}_{O,c} & \boldsymbol{\Xi}_{O,r} \end{bmatrix}. \quad (5)$$

Rewriting Eq. (3) as $\mathcal{M}_O \cdot \mathcal{D}_O = kT\mathbf{I}$, where \mathbf{I} is the identity tensor, one can show that the translation, rotation, and coupling diffusion tensors are related to the friction tensors by [12,18]

$$\mathbf{D}_{O,t} = kT(\boldsymbol{\Xi}_t - \boldsymbol{\Xi}_{O,c}^\dagger \cdot \boldsymbol{\Xi}_{O,r}^{-1} \cdot \boldsymbol{\Xi}_{O,c})^{-1}, \quad (6)$$

$$\mathbf{D}_r = kT(\boldsymbol{\Xi}_{O,r} - \boldsymbol{\Xi}_{O,c} \cdot \boldsymbol{\Xi}_t^{-1} \cdot \boldsymbol{\Xi}_{O,c}^\dagger)^{-1}, \quad (7)$$

$$\mathbf{D}_{O,c} = -kT \boldsymbol{\Xi}_{O,r}^{-1} \cdot \boldsymbol{\Xi}_{O,c} \cdot (\boldsymbol{\Xi}_t - \boldsymbol{\Xi}_{O,c}^\dagger \cdot \boldsymbol{\Xi}_{O,r}^{-1} \cdot \boldsymbol{\Xi}_{O,c})^{-1}. \quad (8)$$

According to Brenner [12], the translation and coupling tensors are most meaningful when computed at the center of diffusion. At this point D , the coupling tensor $\boldsymbol{\Xi}_{D,c}$ is symmetrical. The vector from the origin to the center of diffusion \mathbf{r}_{OD} can be expressed as [12,18]

$$\mathbf{r}_{OD} = \begin{bmatrix} D_r^{22} + D_r^{33} & -D_r^{12} & -D_r^{13} \\ -D_r^{12} & D_r^{11} + D_r^{33} & -D_r^{23} \\ -D_r^{13} & -D_r^{23} & D_r^{11} + D_r^{22} \end{bmatrix}^{-1} \cdot \begin{bmatrix} D_{O,c}^{23} - D_{O,c}^{32} \\ D_{O,c}^{31} - D_{O,c}^{13} \\ D_{O,c}^{12} - D_{O,c}^{21} \end{bmatrix}. \quad (9)$$

The translation and coupling tensors at the center of diffusion are given by

$$\mathbf{D}_t = \mathbf{D}_{O,t} - \mathbf{r}_{OD} \times \mathbf{D}_r \times \mathbf{r}_{OD} + \mathbf{D}_{O,c}^\dagger \times \mathbf{r}_{OD} - \mathbf{r}_{OD} \times \mathbf{D}_{O,c}, \quad (10)$$

$$\mathbf{D}_c = \mathbf{D}_{O,c} + \mathbf{D}_r \times \mathbf{r}_{OD}. \quad (11)$$

Finally, we can write the scalar translational diffusion coefficient as [18]

$$D_t = kT/\zeta_t = \frac{1}{3} \text{Tr}(\mathbf{D}_t), \quad (12)$$

where ζ_t is the translational friction coefficient and $\text{Tr}(\mathbf{D}_t)$ is the trace of the translation diffusion tensor. Similarly, we can define scalar rotational diffusion and friction coefficients as

$$D_r = kT/\zeta_r = \frac{1}{3} \text{Tr}(\mathbf{D}_r). \quad (13)$$

A. Kirkwood-Riseman theory

Based on the preceding discussion, one can fully describe the translational and rotational behavior of a rigid particle, provided one can obtain the translation, rotation, and coupling friction tensors. We will now describe one approach for obtaining those tensors for rigid particles consisting of N spherical elements in the continuum regime. For this discussion, we will consider the case where all N elements have the same radii $a_i = a$, though this need not be the case when applying the general framework described here. We will later discuss how to extend this approach to the transition flow regime.

Kirkwood and Riseman [23] demonstrated that the drag on a particle in continuum flow can be calculated by considering the hydrodynamic interactions between each pair of spheres in the aggregate. Initially, hydrodynamic interactions between spheres were calculated using the Oseen tensor. Later authors introduced more sophisticated hydrodynamic interaction tensors to account for the finite size of the spherical elements [24,25] and for rotational and translation-rotation coupling effects [26–28]. In all of these cases, the relationship between the linear velocity \mathbf{u}_i and angular velocity $\boldsymbol{\omega}_i$ of the i th spherical element and the force \mathbf{F}_j and torque \mathbf{T}_j at the center of each of the N elements is [20]

$$-\mathbf{u}_i = \sum_{j=1}^N \mathbf{Q}_{ij}^t \cdot \mathbf{F}_j + \sum_{j=1}^N (\mathbf{Q}_{ij}^c)^\dagger \cdot \mathbf{T}_j, \quad (14)$$

$$-\boldsymbol{\omega}_i = \sum_{j=1}^N \mathbf{Q}_{ij}^c \cdot \mathbf{F}_j + \sum_{j=1}^N \mathbf{Q}_{ij}^r \cdot \mathbf{T}_j, \quad (15)$$

where \mathbf{Q}_{ij}^t , \mathbf{Q}_{ij}^r , and \mathbf{Q}_{ij}^c are the translation, rotation, and coupling hydrodynamic tensors between the i th and j th spherical elements. These tensors will be defined shortly.

This linear system of equations can be written in matrix form as

$$-\begin{bmatrix} \mathcal{U}_P \\ \mathcal{W} \end{bmatrix} = \begin{bmatrix} \mathbf{Q}^t & (\mathbf{Q}^c)^\dagger \\ \mathbf{Q}^c & \mathbf{Q}^r \end{bmatrix} \begin{bmatrix} \mathcal{F} \\ \mathcal{T}_P \end{bmatrix}, \quad (16)$$

where \mathcal{U}_P , \mathcal{W} , \mathcal{F} , and \mathcal{T}_P are the $3N$ -element vector containing the linear velocities, angular velocities, forces, and torques on the N spherical elements and \mathbf{Q}^t , \mathbf{Q}^r , and \mathbf{Q}^c are the $3N \times 3N$ matrices of the translation, rotation, and coupling tensors for all ij pairs. Note that subscript P indicates that the property is evaluated at the center of each element. For example, the linear velocity of the i th sphere that appears in \mathcal{U}_P is $\mathbf{u}_i = \mathbf{u}_O + \boldsymbol{\omega} \times \mathbf{r}_i$, where $\mathbf{r}_i = (x_i, y_i, z_i)$ is the vector from the origin to the center of the i th element. Inverting Eq. (16), we get

$$\begin{bmatrix} \mathcal{F} \\ \mathcal{T}_P \end{bmatrix} = -\begin{bmatrix} \mathbf{S}^t & (\mathbf{S}^c)^\dagger \\ \mathbf{S}^c & \mathbf{S}^r \end{bmatrix} \begin{bmatrix} \mathcal{U}_P \\ \mathcal{W} \end{bmatrix}, \quad (17)$$

where

$$\begin{bmatrix} \mathbf{S}^t & (\mathbf{S}^c)^\dagger \\ \mathbf{S}^c & \mathbf{S}^r \end{bmatrix} = \begin{bmatrix} \mathbf{Q}^t & (\mathbf{Q}^c)^\dagger \\ \mathbf{Q}^c & \mathbf{Q}^r \end{bmatrix}^{-1}. \quad (18)$$

Carrasco and Garcia de la Torre [20] show that the 3×3 submatrices of the $3N \times 3N$ \mathbf{S} matrices are related to the translation, rotation, and coupling friction tensors in Eqs. (1) and (2) by

$$\boldsymbol{\Xi}_t = \sum_{i=1}^N \sum_{j=1}^N \mathbf{S}_{ij}^t, \quad (19)$$

$$\boldsymbol{\Xi}_{O,r} = \sum_{i=1}^N \sum_{j=1}^N [\mathbf{S}_{ij}^r - \mathbf{S}_{ij}^c \cdot \mathbf{A}_j + \mathbf{A}_i \cdot (\mathbf{S}_{ij}^c)^\dagger - \mathbf{A}_i \cdot \mathbf{S}_{ij}^t \cdot \mathbf{A}_j], \quad (20)$$

$$\boldsymbol{\Xi}_{O,c} = \sum_{i=1}^N \sum_{j=1}^N [\mathbf{S}_{ij}^c + \mathbf{A}_i \cdot \mathbf{S}_{ij}^t], \quad (21)$$

where

$$\mathbf{A}_i = \begin{bmatrix} 0 & -z_i & y_i \\ z_i & 0 & -x_i \\ -y_i & x_i & 0 \end{bmatrix}. \quad (22)$$

Carrasco and Garcia de la Torre [20] summarize the hydrodynamic theories of Reuland *et al.* [26], Mazur and Van Saarloos [27], and Goldstein [28] and show that the hydrodynamic interaction tensors \mathbf{Q}_{ij}^t , \mathbf{Q}_{ij}^r , and \mathbf{Q}_{ij}^c all agree to order r_{ij}^{-3} . These tensors are given by

$$\mathbf{Q}_{ij}^t = \frac{\delta_{ij}}{\zeta_{t,0}} \mathbf{I} + \frac{3(1-\delta_{ij})}{4\zeta_{t,0}} \left[\frac{a}{r_{ij}} \left(\mathbf{I} + \frac{\mathbf{r}_{ij}\mathbf{r}_{ij}}{r_{ij}^2} \right) + \frac{2a^3}{3r_{ij}^3} \left(\mathbf{I} - \frac{3\mathbf{r}_{ij}\mathbf{r}_{ij}}{r_{ij}^2} \right) \right], \quad (23)$$

$$\mathbf{Q}_{ij}^r = \frac{\delta_{ij}}{\zeta_{r,0}} \mathbf{I} + \frac{(1-\delta_{ij})a^3}{2\zeta_{r,0}r_{ij}^3} \left[\frac{3\mathbf{r}_{ij}\mathbf{r}_{ij}}{r_{ij}^2} - \mathbf{I} \right], \quad (24)$$

$$\mathbf{Q}_{ij}^c = -\frac{(1-\delta_{ij})a^3}{\zeta_{r,0}r_{ij}^3} \boldsymbol{\epsilon} \cdot \mathbf{r}_{ij}, \quad (25)$$

where

$$\boldsymbol{\epsilon} \cdot \mathbf{r}_{ij} = \begin{bmatrix} 0 & z_{ij} & -y_{ij} \\ -z_{ij} & 0 & x_{ij} \\ y_{ij} & -x_{ij} & 0 \end{bmatrix}, \quad (26)$$

δ_{ij} is the Kronecker delta and $\zeta_{t,0} = 6\pi\mu a$ and $\zeta_{r,0} = 8\pi\mu a^3$ are the continuum friction and torque coefficients. Note that the second term in Eq. (23) is the Rotne-Prager-Yamakawa tensor [24,25],

$$\mathbf{T}_{ij} = \frac{3}{4\zeta_{t,0}} \left[\frac{a}{r_{ij}} \left(\mathbf{I} + \frac{\mathbf{r}_{ij}\mathbf{r}_{ij}}{r_{ij}^2} \right) + \frac{2a^3}{3r_{ij}^3} \left(\mathbf{I} - \frac{3\mathbf{r}_{ij}\mathbf{r}_{ij}}{r_{ij}^2} \right) \right]. \quad (27)$$

Carrasco and Garcia de la Torre [20] determined that including terms of order lower than r_{ij}^{-3} in the interaction tensors did not significantly improve results for the simple shapes that they analyzed. Since the effect of these lower order terms drop off rapidly for larger particles, we can safely ignore these terms for the larger particles we will consider in this paper.

B. Extension to the transition regime

We now wish to extend this Kirkwood-Riseman framework to the transition flow regime. We start by multiplying Eqs. (14) and (15) by the monomer friction coefficient $\zeta_{t,0}$ and the monomer torque coefficient $\zeta_{r,0}$, respectively. As Rotne and Prager [24] and Yamakawa [25] have noted, the product of the Rotne-Prager-Yamakawa tensor and the Stokes' law friction coefficient is similar to the flow field \mathbf{V}_{ij} around a translating sphere in Stokes flow,

$$\mathbf{v}(\mathbf{r}_{ij}) = \mathbf{V}_{ij} \cdot \mathbf{U}_0, \quad (28)$$

where

$$\mathbf{V}_{ij}(\mathbf{r}_{ij}) = \frac{3}{4} \left[\frac{a}{r_{ij}} \left(\mathbf{I} + \frac{\mathbf{r}_{ij}\mathbf{r}_{ij}}{r_{ij}^2} \right) + \frac{a^3}{3r_{ij}^3} \left(\mathbf{I} - \frac{3\mathbf{r}_{ij}\mathbf{r}_{ij}}{r_{ij}^2} \right) \right]. \quad (29)$$

The difference between \mathbf{V}_{ij} and $\zeta_{t,0}\mathbf{T}_{ij}$ is a factor of 2 in the r_{ij}^{-3} term in $\zeta_{t,0}\mathbf{T}_{ij}$.

Recently, Corson *et al.* [22] exploited the similarity between \mathbf{T}_{ij} and the flow around a sphere to extend Kirkwood-Riseman theory to the transition flow regime by solving for the velocity around a sphere as a function of Knudsen number ($\text{Kn} = \lambda/a$, where λ is the mean free path of molecules in the gas) and substituting the resulting $\mathbf{V}_{ij}(\text{Kn})/\zeta_{t,0}(\text{Kn})$ for the second term in Eq. (23). This gives the drag on the i th element of a purely translating N -element particle as

$$\mathbf{F}_i = -\zeta_{t,0}(\text{Kn})\mathbf{U}_0 - \sum_{j \neq i}^N \mathbf{V}_{ij}(\text{Kn}) \cdot \mathbf{F}_j. \quad (30)$$

In this case, the translation hydrodynamic interaction tensor is given by

$$\mathbf{Q}_{ij}^t(\text{Kn}) = \frac{1}{\zeta_{t,0}(\text{Kn})} [\delta_{ij}\mathbf{I} + (1-\delta_{ij})\mathbf{V}_{ij}(\text{Kn})]. \quad (31)$$

Similarly, we show in Appendix A that the $(1-\delta_{ij})$ terms in the rotation and coupling hydrodynamic interaction tensors are directly related to the flow field around a rotating sphere. Thus, solving for the velocity around and torque on a rotating sphere in the transition flow regime would provide expressions for $\mathbf{Q}_{ij}^r(\text{Kn})$ and $\mathbf{Q}_{ij}^c(\text{Kn})$. This approach should be accurate to order r_{ij}^{-3} , subject to the accuracy of the numerical solution to the kinetic equation in the transition regime and the small error introduced by omitting a factor of 2 in the r_{ij}^{-3} term in the translation hydrodynamic interaction tensor. (These errors are discussed in our previous work [22,29].) To get the friction tensors for a given particle, one would populate and invert the $6N \times 6N$ \mathbf{Q} matrix and apply Eqs. (19)–(21).

Alternatively, one can apply a simplified approach to determine the friction and diffusion tensors for a particle in the transition regime. Ignoring rotation and coupling hydrodynamic interactions, the friction tensors are given by [17,18]

$$\boldsymbol{\Xi}_t = \zeta_{t,0} \sum_{i=1}^N \sum_{j=1}^N \mathbf{S}_{ij}^t, \quad (32)$$

$$\boldsymbol{\Xi}_{o,c} = \zeta_{t,0}(\text{Kn}) \sum_{i=1}^N \sum_{j=1}^N \mathbf{r}_i \times \mathbf{S}_{ij}^t(\text{Kn}), \quad (33)$$

$$\boldsymbol{\Xi}_{o,r} = -\zeta_{t,0} \sum_{i=1}^N \sum_{j=1}^N \mathbf{r}_i \times \mathbf{S}_{ij}^t \times \mathbf{r}_j. \quad (34)$$

Here \mathbf{S}^t is the inverse of the $3N \times 3N$ translation matrix \mathbf{Q}^t rather than a $3N \times 3N$ block of the $6N \times 6N$ \mathbf{Q} matrix in Eq. (16). This approach is equivalent to considering only the linear velocity $\boldsymbol{\omega} \times \mathbf{r}_i$ of each spherical element and ignoring their angular velocities. One obvious flaw of this method is

that it predicts zero torque on a rotating sphere and on a chain of spheres rotating around its long axis. García de la Torre and Rodes [19] suggest adding $N\zeta_{r,0}$ to the diagonal elements of $\Xi_{O,r}$ to partially compensate for this error.

For our transition flow regime calculations, we will apply the simplified approach given by Eqs. (32)–(34). This avoids the need to solve the kinetic equation for a rotating sphere in the transition flow regime and requires inverting a $3N \times 3N$ matrix instead of a $6N \times 6N$ matrix. However, we will apply the volume correction of García de la Torre and Rodes [19] to the rotational friction tensor, using the approximate expression for the ratio of the torque to the free-molecule torque given by Loyalka [30] [Eq. (44) in that work]. As we will demonstrate, the simplified approach is sufficiently accurate for larger particles, for which the $O(r_{ij}^{-3})$ terms in the interaction tensors become less important.

C. Monte Carlo calculations for free-molecule drag and torque

In our previous work [22,29], we compared our results for the translational friction coefficient to published experimental data and analytical results for the transition flow regime. Unfortunately, there is very little information on the rotational diffusion tensor in the transition flow regime. In order to test our extended Kirkwood-Riseman theory, we must compare to results in the continuum and free-molecule limits. Continuum results will be taken from published results in the literature (where available) or obtained using the hydrodynamic interaction tensors given by Eqs. (23)–(25). We now describe our approach for calculating the friction tensors in the free-molecule limit.

Previous authors [31–33] have used a ballistic approach to calculate the drag on a translating particle in free-molecule flow. We use the same approach, but now we consider both translational and rotational motion, and we calculate both the drag and the torque on the particle.

Our procedure is as follows. Consider the general case in which the bulk gas velocity is a combination of translational velocity U_O in the positive x direction and angular velocity ω about the x axis. (For small translational and angular velocities, this is practically equivalent to a particle moving with translational velocity U_O in the negative x direction and rotating with angular velocity $-\omega$, but it is easier to consider the case in which the particle is stationary [30].) Surround the particle by a launch sphere with radius R , randomly select starting locations on the surface of the launch sphere, and define local coordinates (x^*, y^*, z^*) , where x^* is the inward normal for the position on the launch sphere. To determine the momentum of gas molecules leaving the launch sphere, sample from the distribution of velocities of gas molecules entering the launch sphere,

$$f(c_{x^*}, c_{y^*}, c_{z^*}) = K c_{x^*} e^{-[c^* - (U_O + \omega \times \mathbf{R})]^2 / 2\mathcal{R}T}, \quad (35)$$

where $\mathbf{c}^* = (c_{x^*}, c_{y^*}, c_{z^*})$ is molecular velocity in the local coordinate system, \mathcal{R} and T are the gas constant and the gas temperature, the bulk gas velocity $U_O + \omega \times \mathbf{R}$ is written in terms of local coordinates, and K is a normalization constant defined such that

$$\int_0^\infty dc_{x^*} \int_{-\infty}^\infty dc_{y^*} \int_{-\infty}^\infty dc_{z^*} f = 1.$$

If the molecule trajectory intersects the particle, calculate the momentum transfer for diffuse reflection from the surface. For diffuse reflection, the molecule direction is sampled from a cosine-squared distribution for the polar angle and an isotropic distribution for the azimuthal angle, while the molecule speed is sampled from the Maxwell-Boltzmann distribution

$$f(c) = 4\pi \sqrt{\left(\frac{1}{2\pi\mathcal{R}T}\right)^3} c^2 e^{-c^2/2\mathcal{R}T}. \quad (36)$$

Continue to follow the molecule trajectory until it exits the launch and account for multiple collisions between the gas molecule and the particle. After launching M molecules, calculate the total drag and torque on the particle:

$$\mathbf{F} = \frac{A}{M} \sum_{i=1}^M \phi_i \mathbf{p}_i, \quad (37)$$

$$\mathbf{T} = \frac{A}{M} \sum_{i=1}^M \phi_i \mathbf{r}_i \times \mathbf{p}_i. \quad (38)$$

Here A is the launch sphere surface area, \mathbf{p}_i is the momentum transferred to the particle by the i th molecule, and \mathbf{r}_i is the point at which the molecule collides with the particle. The quantity ϕ_i is the flux of gas molecules entering the launch sphere at \mathbf{R}_i [34],

$$\phi_i = n \sqrt{\frac{\mathcal{R}T}{2\pi}} \{e^{-s^2 \cos^2 \theta_i} + \sqrt{\pi} s \cos \theta_i [1 + \text{erf}(s \cos \theta_i)]\}, \quad (39)$$

where n is the gas number density, $s = U/\sqrt{2\mathcal{R}T}$ is the ratio of the bulk velocity to the molecular velocity in the gas, and θ_i is the angle between the bulk velocity and the inward normal to the launch sphere at \mathbf{R}_i .

Using the above procedure, we determine the translation friction tensor by setting the angular velocity of the flow field equal to zero and calculating the drag \mathbf{F}^x , \mathbf{F}^y , and \mathbf{F}^z for flow in the x , y , and z directions. For a translation velocity much less than the thermal speed $\sqrt{2\mathcal{R}T}$, the friction tensor is

$$\Xi_t = \frac{1}{U_O} \begin{bmatrix} F_x^x & F_x^y & F_x^z \\ F_y^x & F_y^y & F_y^z \\ F_z^x & F_z^y & F_z^z \end{bmatrix},$$

where F_x^y signifies the x component of the force on the particle for flow in the y direction. The pure translation calculation (i.e., $\omega = 0$) also gives the coupling tensor from the torque on the particle per Eq. (2). Finally, we calculate the rotation friction tensor by setting the translation velocity to zero and calculating the torque for rotation about the x , y , and z axes.

We have tested our Monte Carlo drag and torque code by comparing our results to published calculation results of Mackowski [33] for the translational friction coefficient (taken as the harmonic average of the eigenvalues of the friction tensor) and by comparing to simple test cases (e.g., a sphere rotating about its center, a sphere rotating about an axis at a fixed distance from its center) for the torque problem. All of our Monte Carlo results are in excellent agreement with results from alternate calculation methodologies. (See Appendix B.) Furthermore, our calculated translation and rotation friction

tensors are symmetrical to within the error in the Monte Carlo calculations. Thus, we can use our Monte Carlo code to evaluate the results of our EKR results in the free-molecule limit.

III. RESULTS

To verify that our extended Kirkwood-Riseman method produces reasonable results across a wide range of Knudsen numbers, we will compare our calculated rotational friction coefficient ζ_r to its values in the continuum and free-molecule limits. We first discuss the continuum and free-molecule results.

A. Continuum regime

Before presenting our results for the rotational friction coefficient in the transition flow regime, it is appropriate to consider the effect of neglecting the rotational and coupling hydrodynamic interaction tensors on ζ_r in the continuum. This issue is discussed in depth in the works of Garcia de la Torre and colleagues (e.g., Refs. [20,21]). We will be using our EKR method to calculate the translation and rotation friction coefficients of a dimer, a linear hexamer, and an octahedral hexamer, so we will briefly discuss the results of Carrasco and Garcia de la Torre [20] for these aggregates. We will also provide continuum results for four different fractal aggregates: $N = 20, d_f = 1.78$; $N = 20, d_f = 2.5$; $N = 100, d_f = 1.78$; and $N = 100, d_f = 2.5$. These aggregates are shown in Fig. 1. Note that these are the same aggregates that we used in our earlier paper [22]. Also note that particles formed by diffusion-limited cluster aggregation processes—such as soot—have a fractal dimension of approximately 1.78.

Carrasco and Garcia de la Torre [20] provide results of various hydrodynamic interaction models for a dimer, linear hexamer, and octahedral hexamer. Our EKR method in the continuum limit is nearly the same as the KRMV (Kirkwood-Riseman with the RPY hydrodynamic interaction tensor and the volume correction to the rotational friction tensor) method described in that paper, with the only difference being the factor of 2 in the $O(r_{ij}^{-3})$ term in \mathbf{Q}_{ij}^r . Presumably, the most accurate computational results are obtained using the shell

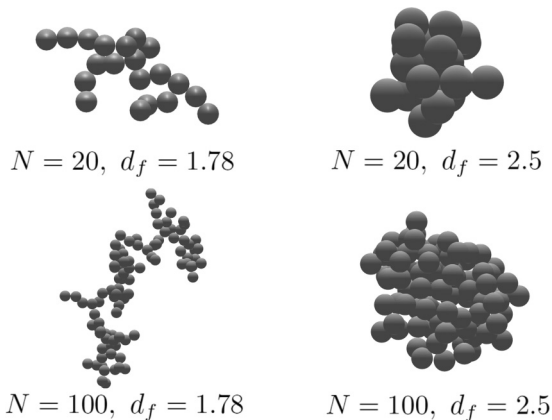


FIG. 1. Representations of the fractal aggregates used in this study.

TABLE I. Continuum friction coefficient for fractal aggregates, normalized by the monomer friction results. Friction coefficients are calculated using terms up to order r_{ij}^{-3} in the hydrodynamic interaction tensors (3RD) or our extended Kirkwood-Riseman theory (EKR) in the continuum limit.

Case	$\zeta_t^{c,3RD}$	$\zeta_t^{c,EKR}$	$\zeta_r^{c,3RD}$	$\zeta_r^{c,EKR}$
$N = 20, d_f = 1.78$	4.35	4.31	94.5	110.8
$N = 100, d_f = 1.78$	10.3	10.2	1292.0	1376.7
$N = 20, d_f = 2.5$	3.41	3.37	42.5	57.5
$N = 100, d_f = 2.5$	6.71	6.64	313.6	398.2

method, where each spherical element in the aggregate is replaced by a large number of frictional units and hydrodynamic interactions are described using the Oseen tensor. We will compare our extended Kirkwood-Riseman results in the continuum limit to the shell method results for the linear and octahedral hexamers. Exact results are available for a dimer in continuum flow [11], so we will compare our extended Kirkwood-Riseman results to the exact values. Based on Table II of Carrasco and Garcia de la Torre [20], we would expect our EKR results to underpredict the translational friction coefficient (or overpredict the translational diffusion coefficient) and overpredict the rotational friction coefficient. We would expect better agreement for less compact aggregates, like linear chains or fractals with $d_f = 1.78$, and better agreement for the translational friction coefficient than for the rotational friction coefficient.

Table I shows translational and rotational friction coefficients for the four fractal aggregates mentioned previously. The table includes ζ_t and ζ_r computed using terms up to order $O(r_{ij}^{-3})$ in the interaction tensors (the 3RD method described by Carrasco and Garcia de la Torre [20]) and using our extended Kirkwood-Riseman method (EKR, where we use the Stokes flow solution around a sphere for the translation interaction tensor and set the coupling and rotation hydrodynamic interaction tensors to zero). Translational friction results are normalized by Stokes' law, $\zeta_{t,0}$; rotational results are normalized to the monomer rotational friction coefficient, $\zeta_{r,0} = 8\pi\mu a^3$.

The difference between $\zeta_t^{c,3RD}$ and $\zeta_t^{c,EKR}$ is small ($<2\%$) for the cases shown here. The difference in the rotational friction coefficient is much larger, with the greatest difference (35%) occurring for $N = 20, d_f = 2.5$. The difference decreases as the average distance between spheres increases due to the reduced importance of the $O(r_{ij}^{-2})$ and $O(r_{ij}^{-3})$ terms in the coupling and rotation interaction tensors, respectively. These trends are consistent with the results of Carrasco and Garcia de la Torre [20] and García de la Torre *et al.* [21].

It is important to note that the 3RD method tends to underpredict the rotational friction coefficient (or overpredict the rotational diffusion coefficient) compared to more computationally intensive methods like the shell model [20,21]. On the other hand, the EKR method appears to overpredict the friction coefficient. In other words, the difference between our EKR results in the continuum and the true value of the rotational friction coefficient may be less than that suggested by the results in Table I. We shall return to this subject in Sec. IV.

TABLE II. Free molecule results for fractal aggregates, normalized by the monomer friction results.

Case	ζ_t^{FM}	ζ_r^{FM}
$N = 2$	1.832	3.829
$N = 6, d_f = 1$	5.056	16.46
$N = 6$, octahedron	4.157	21.57
$N = 20, d_f = 1.78$	14.48	443.9
$N = 100, d_f = 1.78$	64.37	12320
$N = 20, d_f = 2.5$	11.64	196.2
$N = 100, d_f = 2.5$	43.38	2713

B. Free molecule regime

We have computed the free-molecule translational and rotational friction coefficients for the seven aggregates described in the previous section. The results are shown in Table II; the values in the table are normalized to the free-molecule monomer translational and rotational friction coefficients,

$$\zeta_{t,0}^{\text{FM}} = \frac{\pi(8 + \pi)\mu}{2.994\lambda} a^2, \quad (40)$$

$$\zeta_{r,0}^{\text{FM}} = \frac{2\pi\mu}{1.497\lambda} a^4, \quad (41)$$

where we have substituted the viscosity for a hard-sphere gas, $\mu = 0.499\rho\bar{c}\lambda$, into the expressions for $\zeta_{t,0}^{\text{FM}}$ and $\zeta_{r,0}^{\text{FM}}$ [15,35] and assumed diffuse reflection at the surface of the sphere.

Our translation friction coefficient results are in excellent agreement with published computational results for linear chains [31] and for fractals with $d_f = 1.78$ [33]. We are unaware of any published results for the denser particles or for the rotational friction coefficients of any of the particles in Table II.

For our free-molecule calculations, we sample 10^9 molecular trajectories to ensure good statistical results. Each calculation takes less than 3 hours on a single processor, and the CPU time increases linearly with the number of trajectories. In general, our results are accurate to three or four significant figures, based on multiple calculations performed for each case. This level of accuracy is more than sufficient for most practical applications.

C. Transition regime

We have performed our extended Kirkwood-Riseman calculations for the seven particles discussed above for Knudsen numbers ranging from 0.01 to 100. In our previous paper [22], we reported the translational friction coefficient as a function of Knudsen number for the fractal particles, calculated using the harmonic mean of the eigenvalues of the translational friction tensor Ξ_t . The difference between ζ_t computed using this approach and ζ_t computed using Eq. (12) is less than 1%.

Figure 2 presents our results for the scalar rotational friction coefficient ζ_r [defined in Eq. (13)] of a dimer, linear hexamer, and octahedral hexamer. Results are presented as a slip correction factor,

$$C_r(\text{Kn}) \equiv \frac{\zeta_r^c}{\zeta_r^{\text{EKR}}(\text{Kn})}, \quad (42)$$

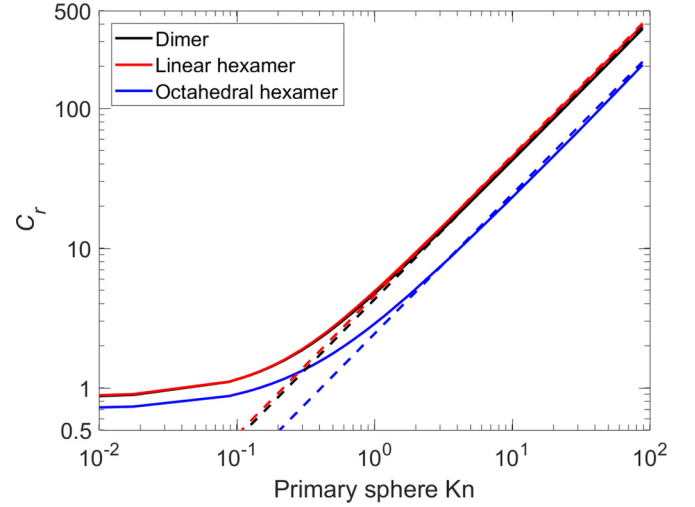


FIG. 2. Calculated rotational slip correction factor [defined by Eq. (42)] for a dimer, linear hexamer, and octahedral hexamer. For the dimer, the continuum value in the slip correction is the exact solution from Happel and Brenner [11]; for the hexamers, the continuum values are the shell method values (SHM) from Table II in Carrasco and Garcia de la Torre [20]. The free-molecule limit for each case (dashed lines) is calculated using our Monte Carlo algorithm.

where the continuum rotational friction coefficient ζ_r^c is calculated using the best available method. (C_r is analogous to the Cunningham slip correction factor, which represents the ratio between Stokes' law and the friction coefficient for a sphere in the transition regime. It is also analogous to the parameter Θ^{-1} , defined by Zhang *et al.* [36] as the ratio of the continuum friction coefficient to the transition regime friction coefficient for an aggregate.) For the dimer, ζ_r^c is given by the exact solution to the Stokes equation [11]; for the hexamers, ζ_r^c is taken as the shell method solution from Carrasco and Garcia de la Torre [20]. The free-molecule limit for each particle is shown as a dashed line. Note that the curves representing the dimer and the linear hexamer nearly coincide due to the chosen normalization used in the plot.

At small Knudsen numbers, the rotational friction coefficient approaches a constant value that differs from the continuum value for the aggregate ζ_r^c because our calculations neglect rotational and coupling hydrodynamic interactions, as discussed in Sec. III A and illustrated by the results in Table I. At large Knudsen numbers, ζ_r^{EKR} is in excellent agreement with our Monte Carlo calculations for the free-molecule rotational friction coefficient (within 5% at $\text{Kn} = 100$). The slight discrepancy between the solid and dashed lines in the free-molecule limit are due to numerical uncertainty in the Monte Carlo calculations and interpolation error in applying our results for the velocity around a sphere to $\mathbf{V}_{ij}(\text{Kn})$ in Eq. (30). (Note that we use a Gaussian quadrature to solve for the velocity within approximately 10 mean free paths of the sphere surface. Thus, interpolation errors are most significant near the free-molecule regime, where the sphere radius is comparable to the node spacing.) These results suggest that rotational and coupling interactions between primary spheres are negligible at large Knudsen numbers, as one would expect due to the nature of free-molecule flow.

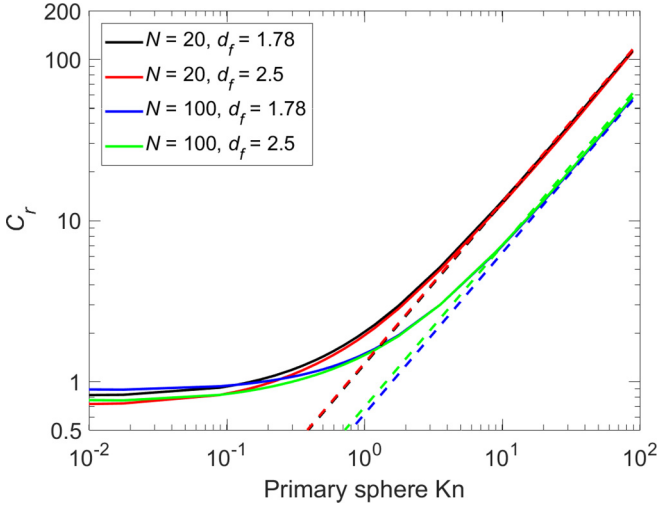


FIG. 3. Calculated rotational slip correction factor [defined by Eq. (42)] for four fractal aggregates. The continuum rotational friction coefficient that appears in the slip correction is calculated using the 3RD method, and the Knudsen-number-dependent friction coefficient is calculated using our EKR method. The free-molecule limit for each aggregate (dashed lines) is calculated using our Monte Carlo algorithm.

Figure 3 presents our results for ζ_r^{EKR} for the fractal particles. Again, the results are plotted as a slip correction factor, but in this case the continuum rotational friction coefficient is calculated using the 3RD method. Note that the two $N = 20$ curves appear to lie on top of each other, as do the two $N = 100$ curves; again, this is due to the chosen normalization.

As with the dimer and hexamers, our results for the fractals are in excellent agreement in the free-molecule limit (dashed line), while the errors in the continuum regime are up to 40% because our method neglects rotational and coupling interactions between monomers. This error decreases significantly for larger, less-dense particles: for example, the difference between our EKR results and the 3RD results for 100-sphere sootlike fractal is less than 10%. The decrease can be attributed to the reduced importance of the $O(r_{ij}^{-2})$ and $O(r_{ij}^{-3})$ terms in the coupling and rotational interaction tensors, respectively, relative to the $O(r_{ij}^{-1})$ term in the translational interaction tensor. For larger, less-dense particles, the monomers are on average spaced further apart than the monomers in a smaller, denser aggregate, such that the translational hydrodynamic interactions dominate.

Dahneke [37] and Zhang *et al.* [36] posited there exists for the translational friction coefficient a universal relationship between the friction coefficient in the transition flow regime and an aggregate Knudsen number,

$$\frac{\zeta_t^c}{\zeta_t(\text{Kn}_{\text{agg}})} = C_c(\text{Kn}_{\text{agg}}), \quad (43)$$

where C_c is the Cunningham slip correction factor. Zhang *et al.* [36] showed using dimensional analysis that the appropriate aggregate Knudsen number for translational friction is

$$\text{Kn}_{\text{agg}} = \frac{\pi \lambda R_H}{\text{PA}}, \quad (44)$$

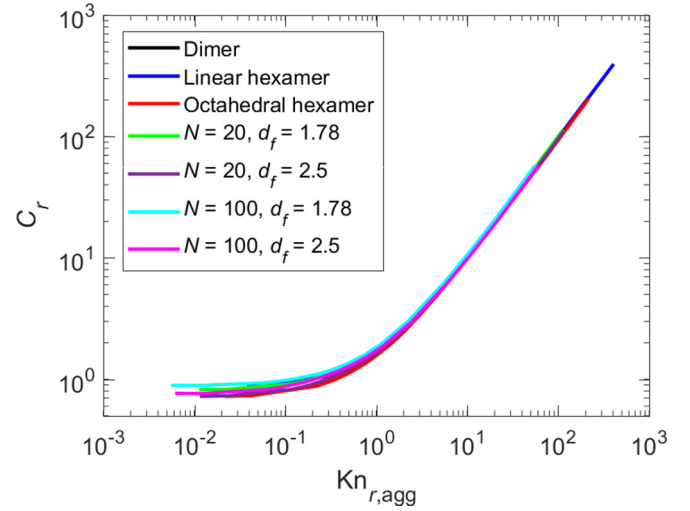


FIG. 4. Rotational slip correction factor plotted versus an aggregate Knudsen number. The aggregate Knudsen number is the ratio of the friction coefficient calculated as if the aggregate is in continuum flow to the friction coefficient calculated as if the aggregate is in free-molecule flow. Continuum friction coefficients are calculated using the same reference method used to calculate the slip correction factor C_r , while the free-molecule coefficients are calculated using our Monte Carlo algorithm.

where R_H and PA are the hydrodynamic radius and projected area of the aggregate, which characterize particle size in the continuum and free-molecule regimes, respectively. In other words, the aggregate Knudsen number is proportional to the ratio between the continuum and free-molecule friction coefficients for the aggregate.

This adjusted sphere method implies that plots of the aggregate translational slip correction factor [Eq. (43)] versus the aggregate Knudsen number [Eq. (44)] fall on the same universal curve, regardless of particle shape. Experimental and computational studies [22,29,36,38,39] suggest that this is indeed the case. Based on this evidence, we propose that the rotational slip correction factor [Eq. (42)] should exhibit similar behavior when plotted against an appropriate aggregate Knudsen number. Since the translational aggregate Knudsen number is proportional to the ratio of continuum to free-molecule friction coefficients, we posit that the rotational aggregate Knudsen number is

$$\text{Kn}_{r,\text{agg}} = \frac{\zeta_r^c}{\zeta_r^{\text{FM}}} = \frac{23.952}{8 + \pi} \frac{\zeta_r^{c*}}{\zeta_r^{\text{FM}*}} \text{Kn}, \quad (45)$$

where Kn is the primary sphere Knudsen number and $\zeta_r^{c*} \equiv \zeta_r^c / \zeta_{r,0}^c$ and $\zeta_r^{\text{FM}*} \equiv \zeta_r^{\text{FM}} / \zeta_{r,0}^{\text{FM}}$ are the dimensionless continuum and free-molecule rotational friction coefficients for the aggregate.

Figure 4 shows our rotational friction coefficient results plotted as the rotational slip correction factor versus the aggregate Knudsen number [Eq. (45)]. The dimensionless continuum friction coefficients are calculated with the same reference method used in Figs. 2 and 3 (i.e., the exact solution for the dimer [11], the shell method for the hexamers [20], and the 3RD method for the 20- and 100-particle aggregates). The dimensionless free-molecule friction coefficients are

calculated using our Monte Carlo algorithm. Roughly speaking, all of the aggregates exhibit the same behavior when plotted in this manner. The differences among the curves near the continuum regime are likely due to neglecting rotational and coupling hydrodynamic interactions when calculating the rotational friction coefficient, as discussed previously. Errors in the calculated continuum friction coefficient may also contribute to the spread among the curves. Our results suggest that the aggregate rotational friction coefficient follows some universal function of the rotational aggregate Knudsen number.

IV. DISCUSSION

We have applied our extended Kirkwood-Riseman theory to calculate the rotational friction coefficient for aerosol particles in the transition flow regime. This approach ignores rotational and translation-rotation coupling interactions between spheres. These effects become less important as the number of primary spheres increase and as the primary sphere size decreases. The former effect is due to the dominance of the $O(r_{ij}^{-1})$ term in the translational interaction tensor over the lower-order terms in the rotational and coupling interaction tensors. The latter effect occurs because smaller particles perturb the flow field less than large particles.

Consistent with this discussion, our EKR results are in excellent agreement with our Monte Carlo results for large Knudsen numbers (i.e., within 5% for $\text{Kn} = 100$). The agreement is not as good in the continuum regime: We have observed errors as high as 40% for dense aggregates relative to the rotational friction coefficient computed considering terms up to order $O(r_{ij}^{-3})$ in the interaction tensors. The EKR results are in better agreement with the 3RD results for less dense fractal aggregates. It is also worth mentioning that the EKR and 3RD methods respectively under- and overpredict the rotational friction coefficient compared to the computationally intensive shell method, so the rotational friction coefficient computed using the EKR method is mostly likely in better agreement with the true friction coefficient than our results in Table I and Fig. 3 suggest.

Our results also suggest that there is a universal relationship between the rotational friction coefficient and an aggregate Knudsen number. This is analogous to relationship between the translational friction coefficient and the aggregate Knudsen number introduced by Dahneke [37] and Zhang *et al.* [36], which is supported by experimental data and computational results [22,29,36,38,39]. For the rotational friction coefficient, the appropriate aggregate Knudsen number is the ratio of the aggregate continuum and free-molecule friction coefficients.

We could improve the accuracy of our method—particularly near the continuum regime—if we considered pairwise rotational and coupling interactions between primary spheres in the aggregate. As we have demonstrated, the rotational and coupling interaction tensors are related to the flow field around a rotating sphere; one could solve the kinetic equation for flow around a rotating sphere as a function of Knudsen number to obtain the appropriate interaction tensors in the transition flow regime. With that said, our simplified method is sufficiently accurate for most practical purposes—particularly for larger aggregates with a fractal dimension of 1.78.

Finally, we will note that while we have focused exclusively on the scalar friction coefficient, our method also provides the translation, rotation, and coupling friction tensors. Thus, our extended Kirkwood-Riseman method can be used when considering alignment of aerosol particles in an external field [3–6,16] or when simulating Brownian diffusion of small particles.

APPENDIX A: RELATIONSHIP BETWEEN THE ROTATION AND COUPLING TENSORS AND THE FLOW AROUND A SPHERE

As mentioned in Sec. II B, the $(1 - \delta_{ij})r_{ij}^{-3}$ and $(1 - \delta_{ij})r_{ij}^{-2}$ terms in the rotation and coupling hydrodynamic interaction tensors are related to the flow around a sphere. We provide the derivation in this appendix. Note that this derivation is similar to the derivation of the lower-order terms in the method of reflections [26,27].

We will start with the rotation hydrodynamic tensor \mathbf{Q}_{ij}^r . Consider a sphere rotating in a quiescent fluid with angular velocity $\boldsymbol{\omega}_j$. This angular motion is sustained by applying a torque $\mathbf{T}_j = \zeta_{r,0}\boldsymbol{\omega}_j$ to the sphere. The velocity induced in the fluid at a location \mathbf{r}_{ij} from the rotating sphere can be written in spherical coordinates as

$$\mathbf{v}(\mathbf{r}_{ij}) = \frac{\omega a^3}{r_{ij}^2} \sin \theta \hat{\mathbf{e}}_\phi, \quad (\text{A1})$$

where $\hat{\mathbf{e}}_\phi$ is the unit vector in the ϕ direction. The vorticity in the fluid is

$$\mathbf{w}(\mathbf{r}_{ij}) = \nabla \times \mathbf{v} = \frac{\omega a^3}{r_{ij}^3} (2 \cos \theta \hat{\mathbf{e}}_r + \sin \theta \hat{\mathbf{e}}_\theta). \quad (\text{A2})$$

Converting to Cartesian coordinates and performing some simple manipulations, we find that the vorticity can be written

$$\mathbf{w}(\mathbf{r}_{ij}) = \frac{a^3}{r_{ij}^3} \left(\frac{3\mathbf{r}_{ij}\mathbf{r}_{ij}}{r_{ij}^2} - \mathbf{I} \right) \cdot \boldsymbol{\omega}_j. \quad (\text{A3})$$

A sphere placed in the fluid at \mathbf{r}_{ij} would rotate with angular velocity $\boldsymbol{\omega}_i = \frac{1}{2}\mathbf{w}(\mathbf{r}_{ij})$ [11], which can be written

$$\boldsymbol{\omega}_i = \left[\frac{1}{2\zeta_{r,0}} \frac{a^3}{r_{ij}^3} \left(\frac{3\mathbf{r}_{ij}\mathbf{r}_{ij}}{r_{ij}^2} - \mathbf{I} \right) \right] \cdot \mathbf{T}_j. \quad (\text{A4})$$

The term in square brackets is the $(1 - \delta_{ij})$ term in the rotation hydrodynamic interaction tensor [Eq. (24)], proving that the rotational interaction between two spheres is related to the vorticity of the flow field around a rotating sphere.

We now turn our attention to the coupling tensor \mathbf{Q}_{ij}^c . Consider a sphere translating through a quiescent fluid with velocity \mathbf{u}_j due to some external force $\mathbf{F}_j = \zeta_{t,0}\mathbf{u}_j$. The vorticity at point \mathbf{r}_{ij} in spherical coordinates is

$$\mathbf{w}_j = -\frac{3}{2} \frac{a}{r_{ij}^2} \mathbf{u}_j \sin \theta \hat{\mathbf{e}}_\phi. \quad (\text{A5})$$

We can write this more generally as

$$\mathbf{w}_j = -\frac{3}{2} \frac{a}{r_{ij}^3} \mathbf{u}_j \times \mathbf{r}_{ij} = \frac{3}{2} \frac{a}{r_{ij}^3} \mathbf{r}_{ij} \times \mathbf{u}_j. \quad (\text{A6})$$

We can write the cross product $\mathbf{r}_{ij} \times \mathbf{u}_j$ as $\mathbf{A}_{ij} \cdot \mathbf{u}_j$, where $\mathbf{A}_{ij} = -\boldsymbol{\epsilon} \cdot \mathbf{r}_{ij}$, such that the vorticity becomes

$$\boldsymbol{\omega}_j = -\left(\frac{3}{2} \frac{a}{r_{ij}^3} \boldsymbol{\epsilon} \cdot \mathbf{r}_{ij}\right) \cdot \mathbf{u}_j. \quad (\text{A7})$$

Again, a sphere placed in the fluid at \mathbf{r}_{ij} would rotate with angular velocity equal to half the vorticity,

$$\boldsymbol{\omega}_j = -\left(\frac{3}{4} \frac{a}{r_{ij}^3} \boldsymbol{\epsilon} \cdot \mathbf{r}_{ij}\right) \cdot \frac{\mathbf{F}_j}{6\pi\mu a}. \quad (\text{A8})$$

Rearranging and introducing $\zeta_{r,0} = 8\pi\mu a^3$, we get

$$\boldsymbol{\omega}_j = \left(-\frac{\boldsymbol{\epsilon} \cdot \mathbf{r}_{ij}}{\zeta_{r,0}} \frac{a^3}{r_{ij}^3}\right) \cdot \mathbf{F}_j. \quad (\text{A9})$$

The term in parentheses is the coupling interaction tensor \mathbf{Q}_{ij}^c given by Eq. (25). This shows that the $O(r_{ij}^{-2})$ term in the translation-rotation coupling interaction tensor is given by the vorticity in the flow field for a translating sphere.

Alternatively, we can derive the coupling tensor by considering the velocity field around a rotating sphere given by Eq. (A1). Writing the velocity using the cross product $\mathbf{r}_{ij} \times \boldsymbol{\omega}_j$ and converting the cross product to $-(\boldsymbol{\epsilon} \cdot \mathbf{r}_{ij}) \cdot \boldsymbol{\omega}_j$, the velocity becomes

$$\mathbf{v}(\mathbf{r}_{ij}) = \frac{a^3}{r_{ij}^3} (\boldsymbol{\epsilon} \cdot \mathbf{r}_{ij}) \cdot \boldsymbol{\omega}_j. \quad (\text{A10})$$

Writing this equation using the torque applied on sphere j to maintain the angular velocity $\boldsymbol{\omega}_j$, we see that the fluid velocity at \mathbf{r}_{ij} is

$$\mathbf{v}(\mathbf{r}_{ij}) = \left(\frac{\boldsymbol{\epsilon} \cdot \mathbf{r}_{ij}}{\zeta_{r,0}} \frac{a^3}{r_{ij}^3}\right) \cdot \mathbf{T}_j. \quad (\text{A11})$$

The term in parentheses is the transpose of \mathbf{Q}_{ij}^c as written in Eq. (25), which shows that the $O(r_{ij}^{-2})$ term in $(\mathbf{Q}_{ij}^c)^\dagger$ is given by the velocity field around a rotating sphere.

APPENDIX B: MONTE CARLO DRAG AND TORQUE RESULTS

We have developed a Monte Carlo algorithm to compute the drag and torque on an N -sphere aggregate in the free-molecule regime. The algorithm is described in Sec. IIC.

Here, we compare the results of our Monte Carlo algorithm to exact results (where available) and to the drag results of Mackowski [33].

1. Drag on a translating sphere

The drag on a sphere in creeping flow in the free-molecule regime \mathbf{F}_0 is given by Epstein's equation [35]. For purely diffuse reflection, our Monte Carlo algorithm gives the drag as $\mathbf{F}_{MC} = 1.001\mathbf{F}_0$, and thus our MC results are in very good agreement with the exact solution.

2. Drag on an aggregate

Mackowski [33] developed a correlation for the drag on a fractal aggregate as a function of the number of monomers N , the fractal dimension d_f , and the fractal prefactor k_0 . The correlation is based on the results of his own Monte Carlo calculations. Using Mackowski's correlation (Eq. (68) of Ref. [33]), the translational friction coefficients, normalized by Epstein's equation, for 20- and 100-sphere aggregates with $d_f = 1.78$ and $k_0 = 1.3$, are 14.15 and 64.23, respectively. In comparison, our Monte Carlo results for the 20- and 100-sphere aggregates with these fractal dimensions are 14.51 and 64.58, respectively. Thus, our MC results are in very good agreement with Mackowski's correlation.

3. Torque on a rotating sphere

Epstein [35] calculates the torque on a sphere rotating about an axis through its center. Using our Monte Carlo algorithm, we get $\mathbf{T}_{MC} = 0.995\mathbf{T}_0$, which is in very good agreement with the exact value.

For a sphere rotating slowly around an axis located a distance R from its center, the magnitude of the torque is given by

$$T = \zeta_{r,0}\omega R^2 + \zeta_{r,0}\omega. \quad (\text{B1})$$

In other words, the torque is the sum of the torque on a sphere rotating about its center with angular velocity ω and the torque due to the linear velocity of the sphere center ωR moving at a distance R from the origin. Our Monte Carlo results for the torque for $R = a$ and $R = 2a$ are $3.763\zeta_{r,0}\omega$ and $12.15\zeta_{r,0}\omega$, respectively, where a is the sphere radius. These results are in very good agreement with the exact results $T = 3.785\zeta_{r,0}\omega$ and $T = 12.14\zeta_{r,0}\omega$ for a sphere rotating around an axis $R = a$ and $R = 2a$ from its center.

[1] C. Sorensen, *Aerosol Sci. Technol.* **45**, 765 (2011).
 [2] M. Li, G. W. Mulholland, and M. R. Zachariah, *Aerosol Sci. Technol.* **46**, 1035 (2012).
 [3] M. Cheng, G. Xie, M. Yang, and D. Shaw, *Aerosol Sci. Technol.* **14**, 74 (1991).
 [4] R. E. Weiss, V. N. Kapustin, and P. V. Hobbs, *J. Geophys. Res. Atmos.* **97**, 14527 (1992).
 [5] I. Colbeck, B. Atkinson, and Y. Johar, *J. Aerosol Sci.* **28**, 715 (1997).

[6] M. Li, G. W. Mulholland, and M. R. Zachariah, *Aerosol Sci. Technol.* **50**, 1003 (2016).
 [7] S.-C. Chen, J. Wang, H. Fissan, and D. Y. H. Pui, *J. Nanopart. Res.* **15**, 1955 (2013).
 [8] C. Branche, P. Schulte, and C. Geraci, Approaches to safe nanotechnology: Managing the health and safety concerns associated with engineered nanomaterials, DHHS (NIOSH) Publication No. 2009-125 (NIOSH, 2009), <https://www.cdc.gov/niosh/docs/2009-125/default.html>.

- [9] A. Albanese, P. S. Tang, and W. C. Chan, *Annu. Rev. Biomed. Eng.* **14**, 1 (2012).
- [10] M. Lattuada, *J. Phys. Chem. B* **116**, 120 (2011).
- [11] J. Happel and H. Brenner, *Low Reynolds Number Hydrodynamics: With Special Applications to Particulate Media*, Prentice-Hall International Series in the Physical and Chemical Engineering Sciences (Prentice-Hall, Eaglewood Cliffs, NJ, 1965).
- [12] H. Brenner, *J. Colloid Interface Sci.* **23**, 407 (1967).
- [13] A. Ortega and J. Garcia de la Torre, *J. Chem. Phys.* **119**, 9914 (2003).
- [14] J. Halbritter, *Z. Naturforsch. A* **29**, 1717 (1974).
- [15] M. M. R. Williams and S. K. Loyalka, *Aerosol Science: Theory and Practice: With Special Applications to the Nuclear Industry* (Pergamon Press, Oxford, 1991).
- [16] M. Li, G. W. Mulholland, and M. R. Zachariah, *Aerosol Sci. Technol.* **48**, 139 (2014).
- [17] J. M. G. Bernal and J. García de La Torre, *Biopolymers* **19**, 751 (1980).
- [18] J. Garcia de La Torre, A. Jimenez, and J. J. Freire, *Macromolecules* **15**, 148 (1982).
- [19] J. García de la Torre and V. Rodes, *J. Chem. Phys.* **79**, 2454 (1983).
- [20] B. Carrasco and J. Garcia de la Torre, *J. Chem. Phys.* **111**, 4817 (1999).
- [21] J. García de la Torre, G. del Rio Echenique, and A. Ortega, *J. Phys. Chem. B* **111**, 955 (2007).
- [22] J. Corson, G. W. Mulholland, and M. R. Zachariah, *Phys. Rev. E* **95**, 013103 (2017).
- [23] J. G. Kirkwood and J. Riseman, *J. Chem. Phys.* **16**, 565 (1948).
- [24] J. Rotne and S. Prager, *J. Chem. Phys.* **50**, 4831 (1969).
- [25] H. Yamakawa, *J. Chem. Phys.* **53**, 436 (1970).
- [26] P. Reuland, B. Felderhof, and R. Jones, *Physica A* **93**, 465 (1978).
- [27] P. Mazur and W. Van Saarloos, *Physica A* **115**, 21 (1982).
- [28] R. F. Goldstein, *J. Chem. Phys.* **83**, 2390 (1985).
- [29] J. Corson, G. W. Mulholland, and M. R. Zachariah, *Aerosol Sci. Technol.* **51**, 766 (2017).
- [30] S. Loyalka, *Phys. Fluids A: Fluid Dynam.* **4**, 1049 (1992).
- [31] P. Chan and B. Dahneke, *J. Appl. Phys.* **52**, 3106 (1981).
- [32] P. Meakin, B. Donn, and G. W. Mulholland, *Langmuir* **5**, 510 (1989).
- [33] D. W. Mackowski, *J. Aerosol Sci.* **37**, 242 (2006).
- [34] G. Bird, *Molecular Gas Dynamics* (Clarendon, Oxford, 1976).
- [35] P. S. Epstein, *Phys. Rev.* **23**, 710 (1924).
- [36] C. Zhang, T. Thajudeen, C. Larriba, T. E. Schwartzentruber, and C. J. Hogan, Jr., *Aerosol Sci. Technol.* **46**, 1065 (2012).
- [37] B. E. Dahneke, *J. Aerosol Sci.* **4**, 163 (1973).
- [38] T. Thajudeen, S. Jeon, and C. J. Hogan, Jr., *J. Aerosol Sci.* **80**, 45 (2015).
- [39] R. Gopalakrishnan, P. H. McMurry, and C. J. Hogan, Jr., *J. Aerosol Sci.* **82**, 24 (2015).